The Astrophysical Journal, 789:163 (7pp), 2014 July 10 doi:10.1088/0004-637X/789/2/163

DIAGNOSTICS OF THE SOLAR CORONA FROM COMPARISON BETWEEN FARADAY ROTATION MEASUREMENTS AND MAGNETOHYDRODYNAMIC SIMULATIONS

G. Le Chat[1,4], J. C. Kasper[2,4,5], O. Cohen[1], and S. R. Spangler[3]
[1] Harvard-Smithsonian Center for Astrophysics, Cambridge, MA, USA; gaetan.lechat@obspm.fr
[2] Atmospheric, Oceanic and Space Sciences Department, University of Michigan, Ann Arbor, MI, USA
[3] Department of Physics and Astronomy, University of Iowa, Iowa City, IA, USA
Received 2013 October 1; accepted 2014 May 23; published 2014 June 25

ABSTRACT

Polarized natural radio sources passing behind the Sun experience Faraday rotation as a consequence of the electron density and magnetic field strength in coronal plasma. Since Faraday rotation is proportional to the product of the density and the component of the magnetic field along the line of sight of the observer, a model is required to interpret the observations and infer coronal structures. Faraday rotation observations have been compared with relatively ad hoc models of the corona. Here for the first time we compare these observations with magnetohydrodynamic (MHD) models of the solar corona driven by measurements of the photospheric magnetic field. We use observations made with the NRAO Very Large Array of 34 polarized radio sources occulted by the solar corona between 5 and 14 solar radii. The measurements were made during 1997 May, and 2005 March and April. We compare the observed Faraday rotation values with values extracted from MHD steady-state simulations of the solar corona. We find that (1) using a synoptic map of the solar magnetic field just one Carrington rotation off produces poorer agreements, meaning that the outer corona changes in the course of one month, even in solar minimum; (2) global MHD models of the solar corona driven by photospheric magnetic field measurements are generally able to reproduce Faraday rotation observations; and (3) some sources show significant disagreement between the model and the observations, which appears to be a function of the proximity of the line of sight to the large-scale heliospheric current sheet.

Key words: magnetohydrodynamics (MHD) – methods: numerical – Sun: corona – Sun: magnetic fields

Online-only material: color figures

1. INTRODUCTION

Magnetic field plays a fundamental role in shaping and heating the solar corona and the solar wind, but due to its weakness and the tenuous nature of coronal plasma, the magnetic field is hard to measure in the outer corona through techniques used closer to the solar surface such as the Zeeman effect. Semi-empirical coronal magnetic field models using the potential field hypothesis (Schatten et al. 1969) can be used to overcome this limitation and determine the magnetic field configuration in the corona and the solar wind. When coupled with a plasma model, such as a magnetohydrodynamic (MHD) simulation, they provide insight on the state of the solar corona and the solar wind, and can investigate the physics of transient phenomena like coronal mass ejections (CME). The ability of such models to simulate the heliosphere up to distances where in situ measurements are available allows direct comparison and validation of the model to a certain extent.

Global models of the solar corona and solar wind have previously been compared with measurements at the photosphere, chromosphere and low corona and in situ at one astronomical unit (e.g., Gibson et al. 1999; Linker et al. 1999; Cohen et al. 2007; Riley et al. 2011). For the first time in this study, comparisons with Faraday rotation measurements have been made to test these models between 5 and 15 $R_\odot$. Faraday rotation measurements come from the effect of a magnetized plasma which rotates the plane of polarization of a linearly polarized radio wave propagating through it. The induced rotation is given by $\Delta\chi = \lambda^2\,\mathrm{RM}$, where $\Delta\chi$ is the change in the polarization position angle, λ is the wavelength of the radio signal and RM is the rotation measure. The rotation measure is given by (in SI units):

$$\mathrm{RM} = \frac{e^3}{8\pi^2\epsilon_0 m_e^2 c^3}\int_{\mathcal{L}} n_e\,\boldsymbol{B}.\boldsymbol{ds} = 2.63\times 10^{-13}\int_{\mathcal{L}} n_e\,\boldsymbol{B}.\boldsymbol{ds}, \quad (1)$$

where n_e is the electron density, $\boldsymbol{B}$ is the magnetic field, $\boldsymbol{ds}$ is the incremental path length vector along the line of sight $\mathcal{L}$, e and m_e are the charge and mass of the electron, ϵ_0 is the permittivity of vacuum, and c is the speed of light. $\Delta\chi$ and RM are signed quantities depending on the direction of the magnetic field along the line of sight: by convention, they are positive when the magnetic field points toward the observer and negative otherwise. $\Delta\chi$ values can become ambiguous (i.e., $\Delta\chi$ may be $\Delta\chi \pm n\times\pi$ rad), therefore the need for multiple frequencies of observation. The density and the magnetic field along the line of sight contribute equally to the value of RM and $\Delta\chi$, consequently they cannot be distinguished by $\Delta\chi$ measurements alone.

Coronal $\Delta\chi$ measurements have been made using background radio sources ranging from spacecraft beacons (Levy et al. 1969; Stelzried et al. 1970; Volland et al. 1977; Levy et al. 1980; Bird et al. 1985; Bird & Edenhofer 1990), extended natural radio sources (Golnev et al. 1964; Sofue et al. 1976; Sakurai & Spangler 1994a, 1994b; Mancuso & Spangler 1999, 2000; Spangler 2005; Ingleby et al. 2007) and pulsars (Bird et al. 1980; Bird 1981; You et al. 2012). Bird (2007) provides an extended review of the coronal $\Delta\chi$ measurements. $\Delta\chi$ measurements have

[4] Also at NASA Lunar Science Institute, Moffet Field, CA, USA.
[5] Also at Harvard-Smithsonian Center for Astrophysics, Cambridge, USA.

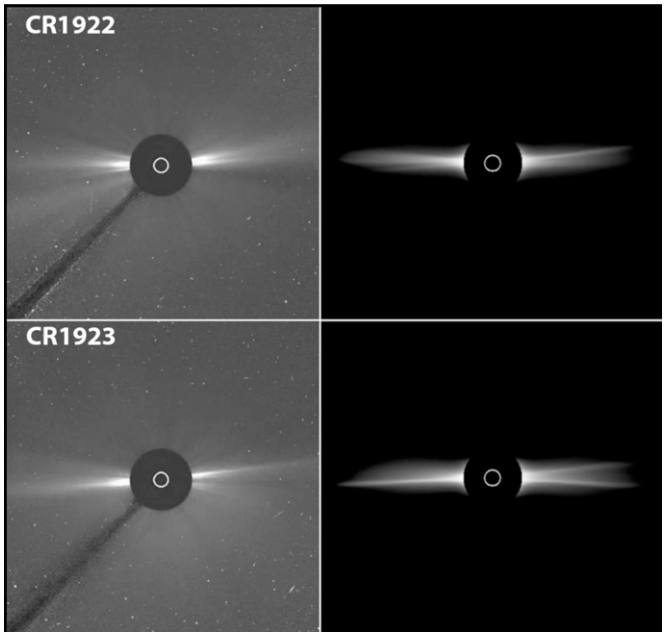

Figure 1. Comparisons of *SOHO*/LASCO C3 images (left) with the model (right) for Carrington rotation numbers 1922 (top) and 1923 (bottom).

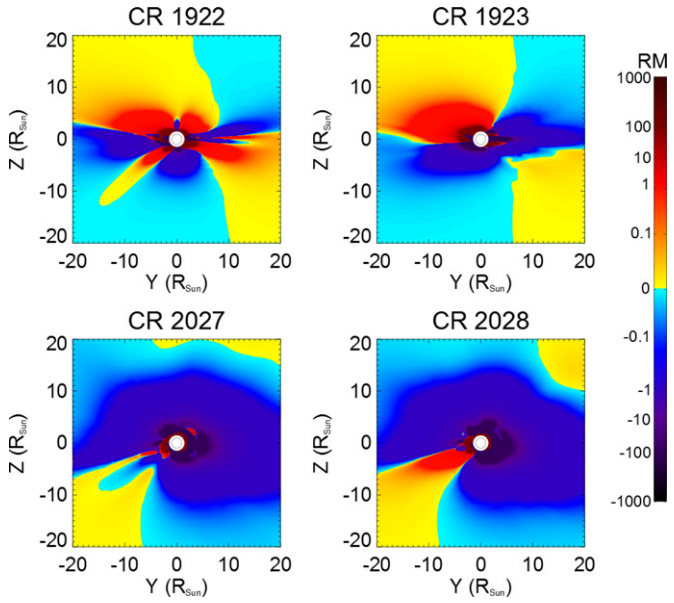

Figure 2. Map of the Faraday rotation obtained from the simulations of Carrington rotation numbers 1922, 1923, 2027, and 2028 for a remote observer in the Sun's equatorial plane. Colors from blue to black correspond to negative RM while colors from yellow to brown correspond to positive RM values.

(A color version of this figure is available in the online journal.)

also been used to study other space and astrophysical plasmas as summarized in a review by Oberoi & Lonsdale (2012).

In this study, we used an existing semi-empirical MHD model to simulate the coronal $\Delta\chi$ (Section 2) and compare the resulting RM to observations previously made at the NRAO Very Large Array (VLA, Section 3). In Section 4, we show results of the comparison and insights into the ability of the model to reproduce the solar corona between 5 and 14 $R_\odot$. We also compare what we can learn from Faraday rotation observations with information from white light coronagraph images collected over the same period.

2. SIMULATIONS

We used the semi-empirical solar corona model developed at the University of Michigan (Roussev et al. 2003; Cohen et al. 2007, 2008). The model is based on the global MHD BATS–R–US code (Powell et al. 1999) and is part of the Space Weather Modeling Framework (Tóth et al. 2005, SWMF). Evaluation of the long-term accuracy of the model and its ability to reproduce coronal and in situ observations was performed by Cohen et al. (2008).

In this model, the additional heating responsible for the high temperature of the corona and the expansion of the solar wind is parameterized by an adjustable value of the ratio of specific heats, γ. The simulation procedure is composed of four steps. First, a potential magnetic field is calculated from magnetogram synoptic maps obtained by the *Solar and Heliospheric Observatory* (*SOHO*)/Michelson Doppler Imager (MDI; Scherrer et al. 1995). This potential field is then used to calculate the distribution of the terminal solar wind speed as a function of the flux tube expansion factor, based on the Wang–Sheeley–Arge model (Wang & Sheeley 1990; Arge & Pizzo 2000). Third, the photospheric boundary conditions for γ and the terminal speed are related by tracing the total energy (Bernoulli Integral) along the flux tubes. Finally, the spatial distribution of γ is specified as a radial function of the photospheric values, and the MHD equations are solved self-consistently until a steady-state with a wind solution is obtained. The density boundary condition used in this model is $n_0 = 1.8 \times 10^{14}\,\mathrm{m}^{-3}$ and the temperature is 3.5×10^6 K in the low corona. The source surface for the magnetic field is at 2.5 $R_\odot$ as commonly defined, and the magnetic field strength is multiplied everywhere by a scaling factor of two, based on comparisons between the model and in situ observations at 1 AU (Cohen et al. 2007).

Figure 1 illustrates how well the model is able to reproduce the observed solar corona and wind by comparing white light images made by the *SOHO*/LASCO C3 coronograph with the model (Lugaz et al. 2005) for Carrington rotation (CR) numbers 1922 and 1923. The model reproduces the streamer belt structures observed in the solar corona, i.e., same number of streams at the same positions and with the same orientations.

Figure 2 shows the Faraday rotation maps obtained from the simulation for CR 1922, 1923, 2027, and 2028, for which observations were made at the VLA (see Section 3). Each map is obtained from the same point of view: a remote observer on the equatorial plane (along the *X*-axis in the Heliocentric Aries Ecliptic coordinates). Comparisons of $\Delta\chi$ maps for adjacent CR illustrate the 27 day evolution of the solar corona and the capability of $\Delta\chi$ measurements to measure it. It also shows one of the limitations of the model based on magnetogram synoptic maps, which use a mean map of the surface field obtained over an entire solar rotation. Consequently, our steady state model assumes that the magnetic field below the source surface doesn't evolve during this period, not taking into account flux emergence or disappearance.

3. OBSERVATIONS

In this study, we use natural continuum radio sources, radio galaxies, and quasars, for measuring the coronal Faraday rotation and comparing it to the model predictions. All observations were made using the NRAO VLA at frequencies of 1465 and 1665 MHz during 1997 May by Mancuso & Spangler (2000)

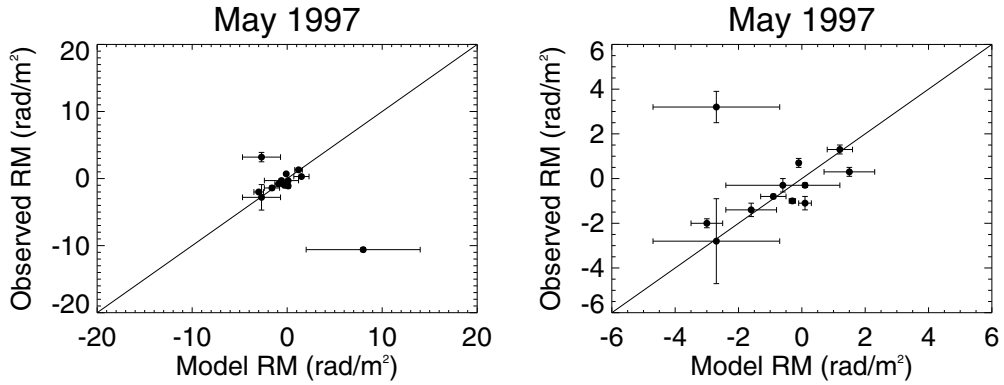

Figure 3. Comparison of observed rotation measures by Mancuso & Spangler (2000) with model rotation measure. The model rotation measure errors are obtained from the variation of the RM values close to the source line of sight. The solid lines represent a perfect agreement between the two. The right panel shows the inner part of the diagram, containing most of the measurements, for which $|\mathrm{RM}| \leqslant 6\,\mathrm{rad\,m^{-2}}$.

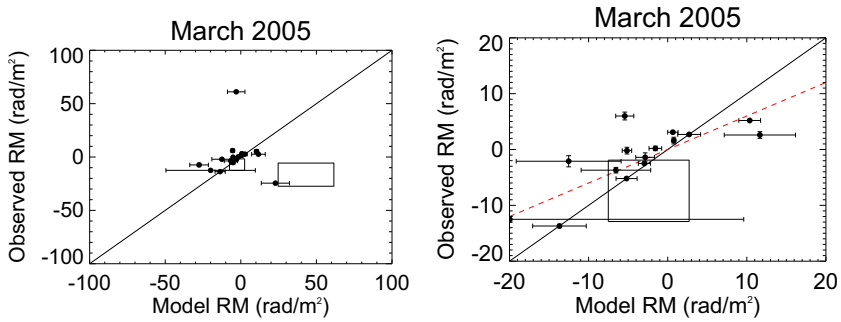

Figure 4. Comparison of observed rotation measures by Ingleby et al. (2007) with model rotation measure. The model rotation measure errors are obtained from the variation of the RM values close to the source line of sight. The solid lines represent a perfect agreement between the two. The right panel shows the inner part of the diagram, containing most of the measurements, for which $|\mathrm{RM}| \leqslant 20\,\mathrm{rad\,m^{-2}}$. The red dashed line corresponds to a linear fit to the data. The square zones correspond to the two sources with large time-variability (see Table 1).

(A color version of this figure is available in the online journal.)

and 2005 March and April by Ingleby et al. (2007). The frequencies chosen have sufficient separation in λ^2 to allow for an accurate determination of the rotation measure, and also to clearly demonstrate the presence of Faraday rotation through its characteristic λ^2 dependence. In both data sets, the radio sources were also observed far from the Sun at the same frequencies. These reference observations gave a polarization position angle, or polarization position angle distributions for extended sources, without the rotation due to the solar corona. These intrinsic, corona-free polarization position angles are determined by the source radiation process (synchrotron radiation), Faraday rotation within the radio source and a surrounding, extragalactic medium, as well as Faraday rotation in the Galactic interstellar medium. Illustrations of data used to obtain the coronal Faraday rotation can be seen in Mancuso & Spangler (2000, Figure 8) and Ingleby et al. (2007, Figure 3). The closest heliocentric distances of the lines of sight analyzed in Mancuso & Spangler (2000) and Ingleby et al. (2007) studies ranged from 5 to 14 $R_\odot$. The position of the observed sources with respect to the Sun can be seen in Mancuso & Spangler (2000, Figure 1) and in Ingleby et al. (2007, Figure 2). Figure 6 shows that the lines of sight come across both fast and slow wind.

The observations and data reduction are described in Mancuso & Spangler (2000) and Ingleby et al. (2007). Table 1 summarizes the observations made in these two previous studies. The total data set consists of 33 observations between 5 and 14 solar radii, with RM values between -27.4 and $+61.1\,\mathrm{rad\,m^{-2}}$. The first 13 observations were made during 1997 May corresponding to CR 1922 and 1923 (Mancuso & Spangler 2000), and the other twenty were made in March and 2005 April during CR 2027 and 2028 (Ingleby et al. 2007). The highest absolute value of RM was made during this second observation period.

4. ROTATION MEASURE COMPARISONS

4.1. Mean Rotation Measure Comparisons

Figures 3 and 4 compare the observed RM values with the ones obtained by the model, for the observations made by Mancuso & Spangler (2000) and by Ingleby et al. (2007), respectively. The solid lines correspond to perfect agreement between the two (i.e., $\mathrm{RM_{obs}} = \mathrm{RM_{model}}$). The general agreement between the observations and the model are good, although there are atypical sources for which the model and the observations significantly disagree.

Our first significant finding is that if we used a synoptic map of the photosphere just one CR off from when the VLA observations were performed, we obtained significantly poorer agreement between the observations and the model. For example, in the 1997 period, the deviation between the observation and the model increased by up to a factor of 10 when the adjacent CR was used as input to the MHD model. This means that the outer solar corona changes in the course of one CR, even in solar minimum, and Faraday rotation observations in the outer corona are sensitive to these changes.

Figure 3 shows good agreement with the observations of Mancuso & Spangler (2000), with a root-mean-square deviation (RMSD) of 5.4 $\mathrm{rad\,m^{-2}}$. A linear regression of the sources with $|\mathrm{RM}| \leqslant 6\,\mathrm{rad\,m^{-2}}$ gives a slope of 0.90 ± 0.03. Nevertheless,

Table 1
Coronal Rotation Measures

Date (UTC)	Source	Carrington Rotation	Distance ($R_\odot$)	RM (rad m^{-2})	Ref
1997 May 6	3C 79	1922	13.84	-1.0 ± 0.1	1
1997 May 6	3C 76.1	1922	7.37	-0.3 ± 0.3	1
1997 May 6	4C+15.09	1922	4.95	$+1.3 \pm 0.2$	1
1997 May 6	4C+20.11	1922	13.41	-0.3 ± 0.1	1
1997 May 11	3C 79	1922	5.96	-10.6 ± 0.3	1
1997 May 11	3C 76.1	1922	12.73	-0.8 ± 0.1	1
1997 May 11	4C+17.15	1922	7.09	$+0.3 \pm 0.2$	1
1997 May 22	4C+18.11	1923	5.79	-1.4 ± 0.3	1
1997 May 22	4C+20.13	1923	8.09	-2.8 ± 1.9	1
1997 May 22	4C+22.06	1923	8.77	-1.1 ± 0.3	1
1997 May 26	3C 114	1923	13.82	$+0.7 \pm 0.2$	1
1997 May 26	4C+20.13	1923	7.76	$+3.2 \pm 0.7$	1
1997 May 26	4C+22.08	1923	7.26	-2.0 ± 0.2	1
2005 March 12	2323–033	2027	7.3	$+61.1 \pm 1.0$	2
2005 March 12	2325–049	2027	8.9	$+6.0 \pm 0.7$	2
2005 March 12	2326–020	2027	5.7	-2.1 ± 1.0	2
2005 March 12	2328–049	2027	7.4	-3.7 ± 0.5	2
2005 March 12	2331–015	2027	6.0	-7.4 ± 1.6	2
2005 March 12	2335–015	2027	7.0	-13.7 ± 0.3	2
2005 March 12	2337–025	2027	6.6	-12.5 ± 0.5	2
2005 March 12	2338–042	2027	8.3	-5.2 ± 0.2	2
2005 March 19	2351–012	2027	5.6	-27.4 to -4.6	2
2005 March 19	2352–016	2027	6.1	-24.5 ± 0.6	2
2005 March 19	2357–024	2027	7.9	$+3.1 \pm 0.2$	2
2005 March 19	0006–001	2027	9.0	$+2.7 \pm 0.2$	2
2005 March 28	0023+045	2028	7.6	$+5.2 \pm 0.1$	2
2005 March 28	0029+052	2028	7.4	-2.5 ± 0.2	2
2005 March 28	0030+058	2028	9.7	$+0.2 \pm 0.4$	2
2005 March 28	0034+013	2028	8.3	$+1.6 \pm 0.6$	2
2005 March 28	0039+033	2028	9.0	$+2.6 \pm 0.6$	2
2005 April 1	0039+033	2028	7.0	-1.4 ± 0.8	2
2005 April 1	0041+070	2028	8.7	-0.2 ± 0.6	2
2005 April 1	0046+062	2028	5.8	-1.9 to -13.3	2

References. (1) Mancuso & Spangler 2000; (2) Ingleby et al. 2007.

there are two notable exceptions: (1) source 4C+20.13 observed on May 26, for which the model gives a negative RM while the observation shows a positive one; and (2) source 3C 79, when it was observed on May 11 with a RM value of -10.6 ± 0.3 rad m^{-2}, the model gives a positive rotation. Without these two sources, the RMSD drops significantly to 0.7 rad m^{-2}. Our result can be compared to the one obtained by Mancuso & Spangler (2000) in which they used a simple model dedicated to Faraday rotation comparison. Their best model for all these observations gives a RMSD of 1.2, which is better that ours since the source 3C 79 is correctly reproduced by their model. However, for the sources with lower absolute RM values, the RMSD of their comparison becomes 1.3, slightly higher than what we obtained using the MHD simulation.

Figure 4 shows the agreement between the model and the observations made by Ingleby et al. (2007). The RMSD is of 22.3. For this data set, three measured RM values differ drastically from the model predictions: (1) source 2323–033 for which the model does not reproduce the large positive RM; (2) source 2351–012 with the large and variable negative RM; and (3) source 2352–016 with a large negative RM value. Without these sources, the RMSD is down to 3.4 rad m^{-2}. A linear regression of the observed RM as a function of the model RM for the sources with $|\mathrm{RM}| \leqslant 20$ rad.m^{-2} gives a slope of 0.60 ± 0.05.

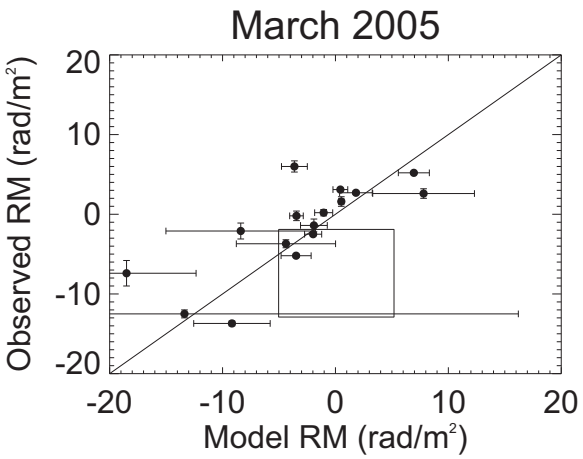

Figure 5. Comparison of observed rotation measures by Ingleby et al. (2007) for which $|\mathrm{RM}| \leqslant 20$ rad m^{-2}, with model rotation measure scaled by a constant factor based on in situ measurements by Issautier et al. (2008) and Smith & Balogh (2008). The solid lines represent a perfect agreement between the two.

It appears that on average the simulation overestimates coronal density and field strength for CR 2027 and 2028.

In situ measurements made during the last solar minimum (Issautier et al. 2008; Smith & Balogh 2008) have shown that both the magnetic field strength and the solar wind density have decreased during the last minimum of activity. In order to reproduce this observed decrease in coronal and solar wind magnetic field strength and electron density, we investigated the impact of reducing the plasma simulations of CR 2027 and 2028 by a constant factor. We started with the reported drop in fast solar wind conditions observed by Ulysses, i.e., a drop of 21% for the electron density (Issautier et al. 2008), and a drop of 15% for the magnetic field strength (Smith & Balogh 2008), leading to a scaling factor of the model RM of 0.67. Figure 5 shows the agreement between the sources with $|\mathrm{RM}| \leqslant 20$ rad m^{-2} and the model the simulated plasma density and field rescaled by a factor of 0.79 and 0.85, respectively based on the observed drop in these parameters (Issautier et al. 2008; Smith & Balogh 2008). Using these rescaled values from the simulations, the RMSD becomes as low as 2.2 rad m^{-2}. This value is similar to the one obtained with the model used by Ingleby et al. (2007), for which the RMSD of the sources with $|\mathrm{RM}| \leqslant 20$ rad.m^{-2} is 2.0 rad m^{-2}.

Figure 6 represents the relative position of the line of sight of the observed radio sources in maps of the solar wind velocity for each CR. The solid lines correspond to the sources for which the RM is well simulated by the model. One can see in Figure 6 that the model is able to reproduce the RM along lines of sight crossing through multiple types of solar wind. The dashed and dashed-dotted lines correspond to the exceptions, which will be discussed in the next subsection.

4.2. Possible Explanations of Anomalous Rotation Measures

The model does not reproduce the RM values of two sources observed by Mancuso & Spangler (2000) in 1997 May: source 4C+20.13 and source 3C 79. The lines of sight of these two exceptions are represented by dashed lines in the two top panels of Figure 6 (source 4C+20.13 was observed during CR 1922, while source 3C 79 was observed during CR 1923). According to Mancuso & Spangler (2000), the value of the rotation measure for source 4C+20.13 had a large error due to strong solar interference. The strong solar interference was due to its vicinity

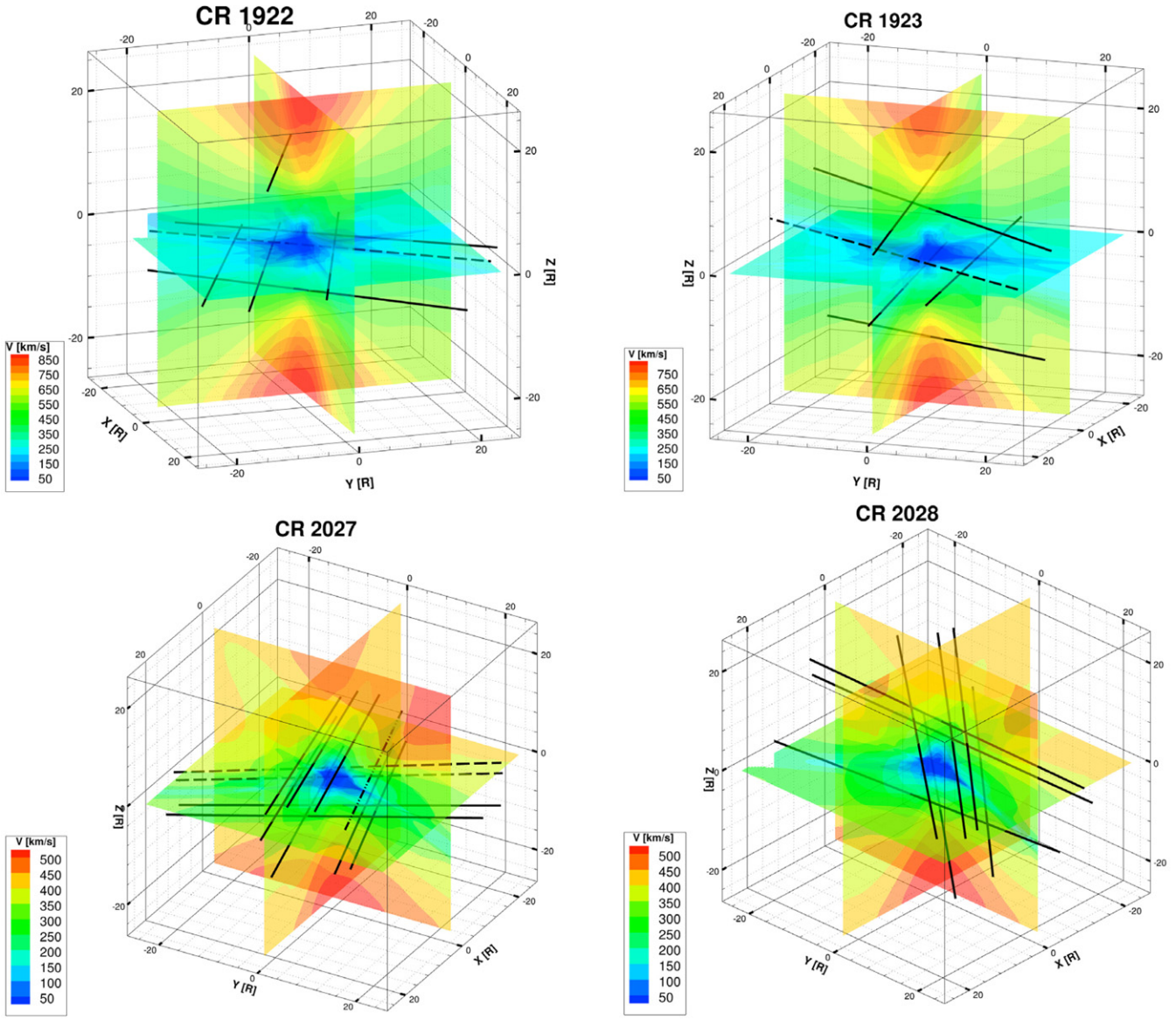

Figure 6. Lines of sight (black lines) of the sources observed during each Carrington rotation, within the solar wind velocity (color maps) obtained by the model of the solar corona. The dashed lines correspond to the sources discussed in Section 4.
(A color version of this figure is available in the online journal.)

to the Sun (7–8 $R_{\odot}$) as well as its location close to the ecliptic, where its line of sight followed a coronal streamer, as shown in Figure 6. From the model point of view, it is noteworthy that the Bernoulli Integral approach used in the third step of the model (Section 2) is not valid in the current sheet, for which the value of γ is forced to approach 1.1 as in the source surface. This may be the origin of the observed disagreement. For source 3C 79, Figure 6 shows also that its line of sight follows a coronal streamer. The model used by Mancuso & Spangler (2000) had a negative RM value for this source, in agreement with observations, by introducing a density asymmetry along the neutral line of the heliospheric current sheet (Mancuso & Spangler 2000, Section 4.4). Such asymmetry may not be reproduced by our MHD model due to the forced value of γ.

From the comparison with the observations by Ingleby et al. (2007), the model failed to reproduce the following sources: source 2323–033, whose line of sight is the dash-dotted line in the bottom left panel of Figure 6, and source 2351–012 and source 2352–016 whose lines-of-sight are plotted using dashed lines. According to Ingleby et al. (2007), whose models did not reproduce the observed RM for these sources either, source 2323–033 is a quasar, which natural variability could be at the origin of the large RM observed. In other words, the polarization angle evolution of this source could have come from an intrinsic polarization variability. It is noteworthy that source 2323–033 is the only source that the model does not reproduce for which the line of sight does not pass through a streamer belt, as shown in Figure 6. For sources 2351–012 and 2352–016, their lines of sight crossed two streamers, as was the case for source 4C+20.13 observed on 1997 May.

4.3. Rotation Measure Fluctuations

In addition to the study of the mean RM of radio sources, Mancuso & Spangler (2000) also provide a study of sources with time-variable coronal Faraday rotation. Figure 7 presents the comparison between the model and the observations of sources 4C+18.11 and 4C+22.06. While the model is able to

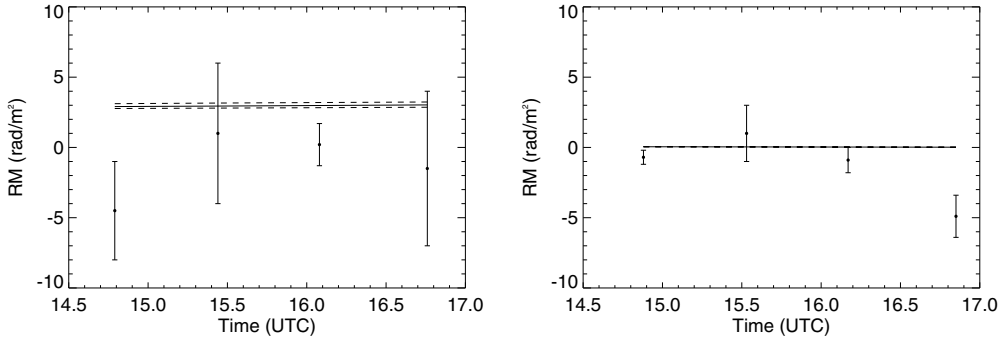

Figure 7. Comparison between the rotation measure time variations observed by Mancuso & Spangler (2000) in 1997 May (plotted points) and the solar corona model (lines) for the following radio galaxies: 4C+18.11 (left) and 4C+22.06 (right).

reproduce the mean RM values, hourly variations observed for these sources are not reproduced by the model. This could come from either small transient events, turbulent motion or waves in the solar corona or from magnetic flux emergence not seen by *SOHO*/MDI while obtaining the synoptic map used by the model. It is usually the case that global models cannot reproduce the RM(t) time series, with the exceptions of some partial successes as shown in Mancuso & Spangler (2000, Figure 7) and in Sakurai & Spangler (1994b). A potential topic for future investigation is the use of an MHD model to subtract the global coronal Faraday rotation signal from observations, permitting the amplitude of fluctuations due to turbulence or other small-scale fluctuations could be quantified.

5. CONCLUSIONS AND PERSPECTIVES

For the first time, we compared coronal Faraday rotation measurements with values extract from an MHD simulation of the solar corona and solar wind driven by measurements of the photospheric field. The measurements were made for lines of sight between 5 and 14 solar radii from the Sun, during a minimum of solar activity (1997 May) and during a declining phase of the solar cycle (2005 March and April).

Our comparison between the simulated and observed mean rotation values leads to the following major results: (1) the coronal Faraday rotation evolves significantly between two following CR (Section 2 and Figure 2); (2) the simulation generally reproduces the large-scale structures of the solar corona, and its boundary conditions may need to be updated from one CR to another (Section 4 and Figures 3 and 4); and (3) the simulation does not seem to be able to reproduce the observed Faraday rotation when the line of sight follows a coronal streamer (Section 4.2 and Figure 6). It may be due to the boundary condition used in the model for the neutral lines which cannot be calculated using the Bernoulli theorem. However, since Faraday rotation is integrated along the line of sight, we cannot pinpoint the origin of these differences. The other possible explanations may be that the large RM values are due to transient structures that are not represented in the CR-averaged input data to the models, or that a small systematic error in the estimation of the density and/or the magnetic field leads to a large difference. This limitation of the model is not apparent when comparing the simulation with white-light coronagraph images, and therefore highlights the unique contribution of Faraday rotation observations for sensing magnetic fields in the outer corona. As a result of this work we highly recommend Faraday rotation measurements be used to validate models of the corona and solar wind.

The results of this comparison are of prime interest for the Solar Probe Plus (SPP) mission, which will for the first time measure in situ the solar atmosphere as close as 9.8 solar radii from the center of the Sun. Coronal simulations have been used to simulate the plasma that the spacecraft and its instruments will encounter. In particular, this model has been used to determine the circumstances under which SPP will cross the Alfvén surface where the solar wind speed is less than the Alfvén speed, $C_A \propto B/n^{1/2}$. In this work we found that our MHD simulation overestimated the product of the density and the magnetic field strength in the outer corona by a factor up to 35% in 2005 March and April before our correction. Since Faraday rotation is a function of the product of density and field we cannot tell if the overestimate is dominated by one of the variables or if it is a combination of the two. Regardless, since the Alfvén speed is a function of both density and magnetic field, the Alfvén speed derived from this model may differ from the coronal value by as much as 35% if the error comes fully from the magnetic field strength, or 10% if the error is more evenly distributed. We therefore caution against relying on numerical simulations for precisely predicting plasma conditions over the orbits of the SPP mission. On the other hand, in situ measurements by SPP, combined with Faraday rotation observations, could dramatically improve the accuracy of these simulations by indicating where the physics need to be improved.

In addition to the model's ability to simulate a steady-state corona, it is widely used to estimate the magnetic field configuration during CME and other coronal events, usually with comparison of extreme ultraviolet observations of the corona (Cohen et al. 2009). Faraday rotation measurements have also been conducted during transient events, for instance using the Helios spacecraft as radio sources (Bird et al. 1985), showing an important modification of the RM as the CME crossed the line of sight, giving important insight of the magnetic field within. Future comparisons between the model and $\Delta\chi$ using recent observations made at the VLA during a CME (Spangler et al. 2013) will be particularly interesting and may give important clues on the physical processes driving the evolution of CMEs from the corona up to the solar wind (Liu et al. 2007).

Finally, new low frequency arrays, like the Murchison Widefield Array, offer the possibility of using multi-source $\Delta\chi$ observations to map the $\Delta\chi$ in the solar corona and may allow prediction of the magnetic polarity (and thus the geoeffectivity) of CMEs directed at Earth (Oberoi & Kasper 2004; Bowman et al. 2007).

Simulation results were obtained using the Space Weather Modeling Framework, developed by the Center for Space

Environment Modeling, at the University of Michigan with funding support from NASA ESS, NASA ESTO-CT, NSF KDI, and DoD MURI. This work was supported at the University of Iowa by grants ATM09-56901 and AST09-07911 from the National Science Foundation.

REFERENCES

Arge, C. N., & Pizzo, V. J. 2000, JGRA, 105, 10465
Bird, M. K. 1981, in Solar Wind Four [MPAE-W-100-81-31], ed. H. Rosenbauer (Garching: Max-Planck-Institute für Aeronomie), 78
Bird, M. K. 2007, A&AT, 26, 6, 441
Bird, M. K., & Edenhofer, P. 1990, in Physics of the Inner Heliosphere, ed. R. Schwenn & E. Marsch (Berlin: Springer), 13
Bird, M. K., Schrfer, E., Volland, H., & Sieber, W. 1980, Natur, 283, 459
Bird, M. K., Volland, H., Howard, R. A., et al. 1985, SoPh, 98, 341
Bowman, J. D., Cairns, I., Kaplan, D. L., et al. 2013, PASA, 30, 31
Cohen, O., Attrill, G. D. R., Manchester, W. B., IV, & Wills-Davey, M. J. 2009, ApJ, 705, 587
Cohen, O., Sokolov, I. V., Roussev, I. I., & Gombosi, T. I. 2008, JGRA, 113, 3104
Cohen, O., Sokolov, I. V., Roussev, I. I., et al. 2007, ApJL, 654, L163
Gibson, S. E., Biesecker, D., Guhathakurta, M., et al. 1999, ApJ, 520, 871
Golnev, V. Y., Pariiskii, Y. N., & Soboleva, N. S. 1964, IzPul, 23, 22
Ingleby, L. D., Spangler, S. R., & Whiting, C. A. 2007, ApJ, 668, 520
Issautier, K., Le Chat, G., Meyer-Vernet, N., et al. 2008, GeoRL, 35, L19101
Levy, G. S., Sato, T., Seidel, B. L., et al. 1969, Sci, 166, 596
Levy, G. S., Volland, H., Bird, M. K., Stelzried, C. T., & Seidel, B. L. 1980, in The HELIOS Solar Probes: Science Summaries [NASA-TM 82005], ed. J. H. Trainor (Greenbelt, MD: Goddard Space Flight Center), 85
Linker, J. A., Mikić, Z., Biesecker, D. A., et al. 1999, JGR, 104, 9809
Liu, Y., Manchester, W. B., IV, Kasper, J. C., Richardson, J. D., & Belcher, J. W. 2007, ApJ, 665, 1439
Lugaz, N., Manchester, W. B., IV, & Gombosi, T. I. 2005, ApJ, 627, 1019
Mancuso, S., & Spangler, S. R. 1999, ApJ, 525, 195
Mancuso, S., & Spangler, S. R. 2000, ApJ, 539, 480
Oberoi, D., & Kasper, J. C. 2004, P&SS, 52, 1415
Oberoi, D., & Lonsdale, C. J. 2012, RaSc, 47, RS0K08
Powell, K. G., Roe, P. L., Linde, T. J., Gombosi, T. I., & De Zeeuw, D. L. 1999, JCoPh, 154, 284
Riley, P., Lionello, R., Linker, J. A., et al. 2011, SoPh, 274, 361
Roussev, I. I., Forbes, T. G., Gombosi, T. I., et al. 2003, ApJ, 588, L45
Sakurai, T., & Spangler, S. R. 1994a, RaSc, 29, 635
Sakurai, T., & Spangler, S. R. 1994b, ApJ, 434, 773
Schatten, K. H., Wilcox, J. M., & Ness, N. F. 1969, SoPh, 6, 442
Scherrer, P. H., Bogart, R. S., Bush, R. I., et al. 1995, SoPh, 162, 129
Smith, E. J., & Balogh, A. 2008, GeoRL, 35, L22103
Sofue, Y., Kawabata, K., Takahashi, F., & Kawajiri, N. 1976, SoPh, 50, 465
Spangler, S. R. 2005, SSRv, 121, 189
Spangler, S. R., Fischer, P. D., Kooi, J. E., & Buffo, J. J. 2013, AAS/SPD, 44, 15
Stelzried, C. T., Levy, G. S., Sato, T., et al. 1970, SoPh, 14, 440
Tóth, G., Sokolov, I. V., Gombosi, T. I., et al. 2005, JGR, 110, A12226
Volland, H., Bird, M. K., Levy, G. S., Stelzried, C. T., & Seidel, B. L. 1977, J. Geophys., 42, 659
Wang, Y.-M., & Sheeley, N. R. 1990, ApJ, 355, 726
You, X. P., Coles, W. A., Hobbs, G. B., & Manchester, R. N. 2012, MNRAS, 422, 1160